

# Griffiths phase and critical behavior in layered $\text{Sr}_2\text{IrO}_4$ ferromagnet

A. Rathi<sup>a,b</sup>, Sonam Perween<sup>a,b</sup>, P. K. Rout<sup>a</sup>, R. P. Singh<sup>c</sup>, Anurag Gupta<sup>a,b</sup>, Sukhvir Singh<sup>a,b</sup>, B. Gahtori<sup>a,b</sup>, B. Sivaiah<sup>a,b</sup>, Ajay Dhar<sup>a,b</sup>, A. K. Shukla<sup>a,b</sup>, R. K. Rakshit<sup>a,b</sup>, R. P. Pant<sup>a,b</sup> and G. A. Basheed<sup>a,b,†</sup>

<sup>a</sup>CSIR-National Physical Laboratory (NPL), Dr. K. S. Krishnan Marg, New Delhi - 110012, India

<sup>b</sup>Academy of Scientific and Innovative Research (AcSIR), NPL Campus, New Delhi - 110012, India

<sup>c</sup>Department of Physics, Indian Institute of Science Education and Research (IISER) Bhopal, Bhopal-462 023, India\*

We report the existence of Griffiths phase (GP) and its influence on critical phenomena in layered  $\text{Sr}_2\text{IrO}_4$  ferromagnet ( $T_C = 221.5$  K). The power law behavior of inverse magnetic susceptibility,  $1/\chi(T)$  with exponent  $\lambda = 0.18(2)$  confirm the GP in the regime  $T_C < T \leq T_G = 279.0(5)$  K. Moreover, the detailed critical analysis via modified Arrott plot method exhibits unrealistic critical exponents  $\beta = 0.77(1)$ ,  $\gamma = 1.59(2)$  and  $\delta = 3.06(4)$ , in corroboration with magneto-caloric study. The abnormal exponent values have been viewed in context of *ferromagnetic-Griffiths* phase transition. The GP has been further analyzed using Bray model, which yields a reliable value of  $\beta = 0.19(2)$ , belonging to the two-dimensional (2D)  $XYh_4$  universality class with strong anisotropy present in  $\text{Sr}_2\text{IrO}_4$ . The present study proposes Bray model as a possible tool to investigate the critical behavior for Griffiths ferromagnets in place of conventional Arrott plot analysis. The possible origins of GP and its correlation with insulating nature of  $\text{Sr}_2\text{IrO}_4$  have been discussed.

*Keywords:* 5d iridates, Griffiths phase, Critical phenomena.

## I. INTRODUCTION

The Ir-based 5d transition metal oxides (TMOs) are widely known to exhibit various unconventional and novel properties [1–3], driven by strong spin-orbit coupling (SOC). The spatially extended nature of 5d electrons in these oxides results in weak (compared to 3d TMOs) electronic correlations and a metallic paramagnetic (PM) behavior is anticipated. In contrast, many iridates [4, 5] happen to be magnetic insulators due to large SOC present in the system. In particular, the layered iridate  $\text{Sr}_2\text{IrO}_4$  (SIO) has emerged as an interesting system due to its structural [5] and magnetic [1] similarities with the novel layered cuprate spin-1/2 Heisenberg antiferromagnet (AFM)  $\text{La}_2\text{CuO}_4$ . The large SOC ( $\sim 0.4$  eV) in SIO splits the  $\text{Ir}^{4+}$  ( $d^5$ )  $t_{2g}$  level into Kramer's doublet with a filled  $J_{eff} = 3/2$  low energy state and a half filled effective  $J_{eff} = 1/2$  high energy state [6], which makes the system different from the spin-1/2  $\text{La}_2\text{CuO}_4$ .

The SIO crystallizes in a tetragonal crystal structure with an arrangement of two-dimensional (2D)  $\text{IrO}_2$  layers along the c-axis, as in  $\text{La}_2\text{CuO}_4$ , but with the rotation of  $\text{IrO}_6$  octahedra around c axis by  $\sim 11^\circ$  [5, 7]. This rotation breaks the inversion symmetry of in-plane Ir-O-Ir network and Dzyaloshinsky-Moriya (DM) interaction between  $J_{eff} = 1/2$  spins gives rise to a weak ferromagnetic (FM) order below  $T_C \sim 230$  K with a moment of  $\sim 0.14 \mu_B/\text{Ir}$  within each  $\text{IrO}_2$  (basal ab-) plane [5, 8]. The system otherwise would behave like a collinear AFM, as  $\text{La}_2\text{CuO}_4$ . Furthermore, the X-ray resonant magnetic scattering (XRMS) studies on SIO established the correlation between  $J_{eff}$  spins in PM state [9, 10]. This often

leads to “*Griffiths singularity*” [11, 12], which is characterized by the presence of short-range FM clusters above Curie temperature.

Griffiths [11], originally, proposed the “*Griffiths singularity*” to explain the role of quenched randomness in diluted Ising ferromagnets. Bray et al. [13, 14] generalized the argument for any disordered system, where intrinsic disorder breaks the system into short-range FM clusters of different sizes with each one having its own Curie temperature,  $T_C(p)$ , where p is the degree of disorder. The long-range FM order is established only below a threshold disorder,  $p_C$  at a much lower temperature,  $T_C^R$  compared to the zero disorder system Curie temperature,  $T_G$ , the Griffiths temperature. The temperature regime,  $T_C^R < T_C(p) \leq T_G(p=0)$ , in which the singularity exists, is usually referred to the Griffiths phase (GP).

Here, for the first time, we report Griffiths phase in layered  $\text{Sr}_2\text{IrO}_4$  ferromagnet. The essential requirement for realization of GP is the absence of long-range order, which can be confirmed through critical phenomena analysis. In this paper, we present the critical behavior across the *ferromagnetic-Griffiths* phase transition in  $\text{Sr}_2\text{IrO}_4$  via *dc* magnetization measurements. The basic difference between pure (conventional) and Griffiths ferromagnets lies in their free energy expression across the phase transition; the former has an analytic free energy expression while the expression for later is non-analytic [11]. The non-analytic nature of GP leads to unrealistically large critical exponents [15–17] through modified *Arrott* plot, scaling law and magneto-caloric analysis. Here, we utilize Bray model to investigate the critical behavior of  $\text{Sr}_2\text{IrO}_4$ . The present study proposes Bray model as a possible tool to investigate the critical behavior for Griffiths ferromagnets. We also discuss the possible origin of insulating nature of  $\text{Sr}_2\text{IrO}_4$  in the context of GP.

\*†basheedga@nplindia.org

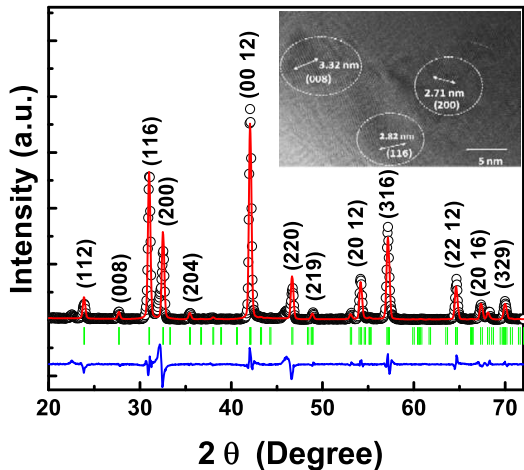


FIG. 1: Room temperature X-ray diffraction pattern (open circles) of  $\text{Sr}_2\text{IrO}_4$ , along with the full-profile (Rietveld) fit (solid red line). The difference between observed and calculated data is shown by solid blue line. The vertical bars show the position of allowed (hkl) Bragg reflections. The inset shows the HRTEM image of  $\text{Sr}_2\text{IrO}_4$ .

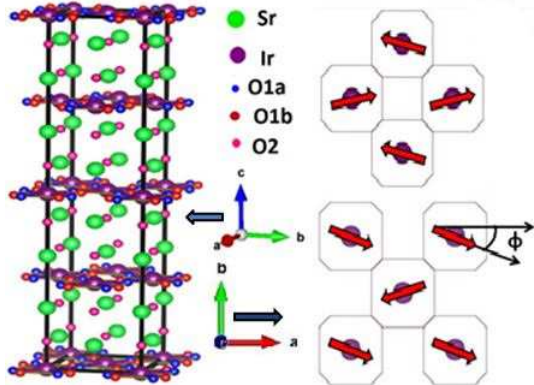


FIG. 2: The left panel shows the layered perovskite structure of  $\text{Sr}_2\text{IrO}_4$ . The right panel shows the schematic magnetic structure of  $\text{Sr}_2\text{IrO}_4$  with the clockwise and anticlockwise rotation of alternate basal (ab) planes around c-axis by  $\phi \sim 11^\circ$ .

## II. EXPERIMENTAL DETAILS

The  $\text{Sr}_2\text{IrO}_4$  polycrystalline sample was synthesized through solid state reaction method. The starting oxides  $\text{SrCO}_3$  (99.99% purity) and  $\text{IrO}_2$  (99.99% purity) were mixed in stoichiometric ratio. The mixture was heated in air at 800, 900 and 1000°C for 12 hours each with intermediate grindings. Finally, the mixture was pressed into pellet and sintered at 1000°C for 24 hours. The phase quality of the sample was examined using a four-circle high resolution X-ray diffractometer (Cu- $K_\alpha$  radiation). Figure 1 shows the room temperature X-ray diffraction pattern of  $\text{Sr}_2\text{IrO}_4$ , along with the profile (Rietveld) fit using FULLPROF program. The Rietveld fit confirms the single tetragonal phase (space group  $I4_1/acd$ ) with the refined lattice parameters,  $a = 5.50 \text{ \AA}$ ,  $b = 5.50 \text{ \AA}$  and  $c = 25.76 \text{ \AA}$ , which are in close agreement with earlier reports on SIO [5, 7]. The inset of Fig. 1 shows the HRTEM image of as synthesized SIO sample which

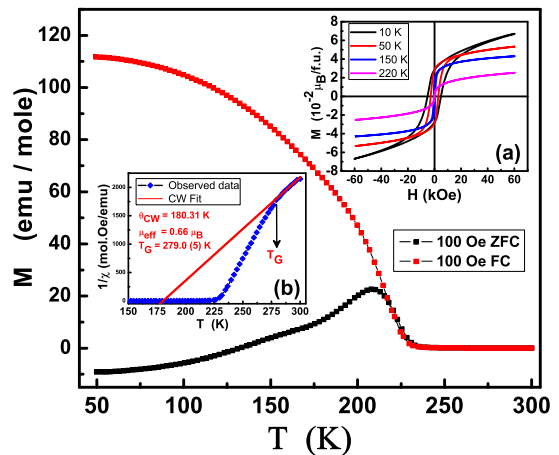


FIG. 3: The temperature dependence of dc magnetization in FC and ZFC modes at 100 Oe. Inset (a) shows the MH loops observed at different temperatures. Inset (b) shows  $1/\chi(T)$  plot along with Curie-Weiss law fit.

clearly reveals (008), (116) and (200) atomic planes which further confirms high crystallinity of  $\text{Sr}_2\text{IrO}_4$  sample. The Rietveld fit was further used to generate the crystal structure and (schematic) magnetic structure. The left panel of Fig. 2 shows the layered perovskite structure of  $\text{Sr}_2\text{IrO}_4$ , while the right panel reveals the magnetic structure with rotation of  $\phi \sim 11^\circ$  of alternate basal (ab) planes around c axis, in clockwise and anticlockwise direction, respectively. The magnetic properties were investigated by measuring the detailed dc magnetization,  $M(H, T)$ , using SQUID magnetometer. Furthermore, the magnetic isotherms were recorded in the vicinity of critical temperature using a Quantum Design PPMS.

## III. RESULT AND DISCUSSION

### A. dc magnetization

Figure 3 shows the temperature dependence of dc magnetization measured in the field-cooled (FC) and zero-field-cooled (ZFC) modes at 100 Oe. The plot shows the sharp increase in magnetization below  $T_C \sim 220 \text{ K}$ , which is in close agreement with earlier reports [5, 18, 19]. On cooling, the bifurcation between FC and ZFC magnetization appears, along with a broad maxima in ZFC magnetization, which suggests a large magnetic anisotropy in the system. On further cooling, the dc magnetization shows minor AFM transition at  $\sim 160 \text{ K}$ , which is consistent with earlier reports on SIO [19, 20]. Moreover, the AFM transition weakens with the increasing field and suppresses in a high field of 1 T (not shown here), which can be associated with domination of FM moment over AFM moment in high fields. The inset (a) in Fig. 3 shows the MH loops measured at different temperatures with a field range of  $\pm 6 \text{ T}$ . The loop at 10 K shows the non-saturating behavior with a magnetization value of  $\mu_H = 0.07 \mu_B/\text{f.u.}$  at 6 T. The observed  $\mu_H$  value is consistent with earlier reports [19], however,

much smaller compared to the theoretical value,  $\mu_H = g J_{eff} \mu_B = 0.33 \mu_B/\text{f.u.}$  with  $J_{eff} = 1/2$  and  $g_J = 2/3$ . The non-saturating behaviour and very small  $\mu_H$  value confirm the presence of low temperature AFM component. Moreover, the observed high remanance ( $M_R \sim 0.028 \mu_B/\text{f.u.}$ ) and coercivity ( $H_C \sim 5.20 \text{ kOe}$ ) at 10 K confirm large magnetic anisotropy present in the system. The MH loops observed at higher temperatures, from 50 K to 220 K show that the saturating behavior increases with increase in temperature due to the lowering of AFM contribution.

The inset (b) in Fig. 3 shows the temperature dependence of inverse magnetic susceptibility ( $1/\chi$ ) at 100 Oe. The high temperature data, fitted with the Curie-Weiss (CW) equation,  $\chi = C/(T - \theta_{CW})$ , gives  $\theta_{CW} = +180.31$  K and  $\mu_{eff} = 0.66 \mu_B$ . The positive  $\theta_{CW}$  value confirms the FM ordering, whereas the obtained  $\mu_{eff}$  value exceeds the theoretical value  $\mu_{eff} = g_J \sqrt{J_{eff}(J_{eff} + 1)} = 0.57 \mu_B/\text{f.u.}$  More importantly, the  $1/\chi$  (T) plot shows the negative deviation from the CW behavior much above  $T_C \sim 220$  K. The negative downturn in  $1/\chi$  plot above  $T_C$  and the larger experimental  $\mu_{eff}$  value suggest the formation of short range magnetic clusters in PM state, which is a signature of Griffiths singularity [12, 21]. The Griffiths temperature can be determined as  $T_G = 279.0(5)$  K and the temperature range of GP with respect to pure FM phase is calculated as  $\% = (T_G - T_C)/T_C \times 100$  which comes out to be 26.8 %. The GP has been discussed in more detail in section III (C).

## B. Critical phenomena

The basic feature of GP is the absence of long-range magnetic order in the system, which can be examined through Arrott plot analysis. Figure 4(a) shows the  $M$  ( $H$ ) isotherms at different temperatures around  $T_C$ , ranging from 205 K to 239 K with a temperature interval of 3 K. All the isotherms show non-linear and non-saturating behavior up to 6 T, indicating the presence of short-range FM order [22]. The inset in Fig. 4(a) shows the  $-dM/dT$  versus temperature plot at 250 Oe, revealing the  $T_C$  value, lying between 220 and 223 K. Figure 4(b) shows the basic Arrott plots [23];  $M^2$  against  $H/M$  (Mean field model [24]) for the temperatures near  $T_C$ . The Arrott plots have positive slope, which confirms the second-order magnetic phase transition (SOPT), according to Banerjee's criteria [25]. Furthermore, a series of parallel and straight lines are expected for high field data in Arrott plot, however, the plots show a non-linear diverging behaviour with increasing magnetic field. The breakdown of long-range mean field model supports the presence of Griffiths phase. Therefore, the modified Arrott plot (MAP) method has been used, which is based on the Arrott-Noakes equation,  $(H/M)^{1/\gamma} = (T - T_C)/T_1 + (M/M_1)^{1/\beta}$ , where  $\beta$  and  $\gamma$  are the critical exponents;  $T_1$  and  $M_1$  are constants [26]. The two critical exponents are further related

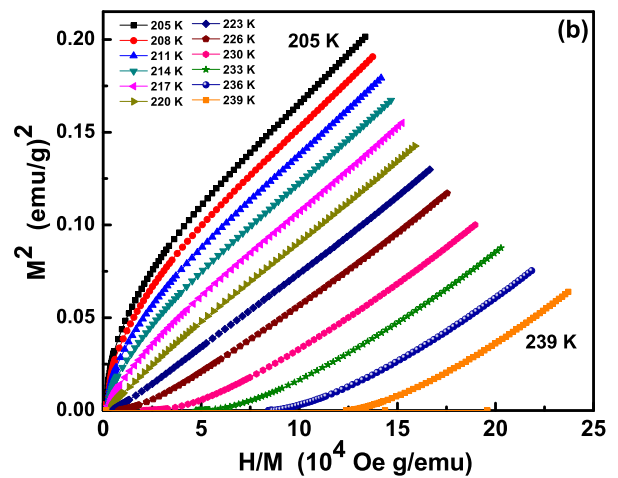
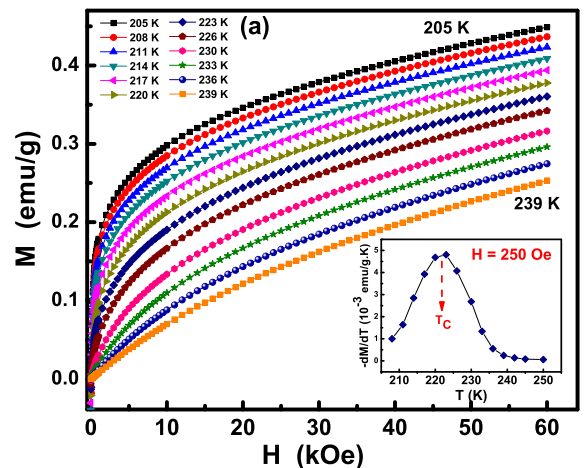


FIG. 4: (a) The magnetic isotherms at different temperatures around  $T_C$ . The inset shows the  $-dM/dT$  versus  $T$  plot at 250 Oe, showing magnetic transition at  $220 \text{ K} \leq T_C \leq 223 \text{ K}$ . (b) The basic Arrott plot;  $M^2$  against  $H/M$  (Mean field model,  $\beta = 0.5$  and  $\gamma = 1.0$ ) at different temperatures around  $T_C$ .

through Widom scaling relation,  $\delta = 1 + \gamma/\beta$  [27] where  $\delta$  is third critical exponent. The modified Arrott plots;  $M^{1/\beta}$  against  $(H/M)^{1/\gamma}$  were constructed using critical exponents for different known universality classes (Table I). However, the plots (not shown here) do not show the expected parallel and straight lines, excluding their validity for SIO system and hence, a detailed critical analysis is required.

For a SOPT, the critical exponents ( $\beta$ ,  $\gamma$  and  $\delta$ ) can be determined from the spontaneous magnetization,  $M_S$  ( $T < T_C$ ), initial susceptibility,  $\chi_0$  ( $T > T_C$ ) and the critical isotherm,  $M(H, T_C)$  asymptotic relations [26],

$$M_S(T) = M_0(-\epsilon)^\beta, \quad T < T_C \quad (1)$$

$$1/\chi_0 = (h_0/M_0)(\epsilon)^\gamma, \quad T > T_C \quad (2)$$

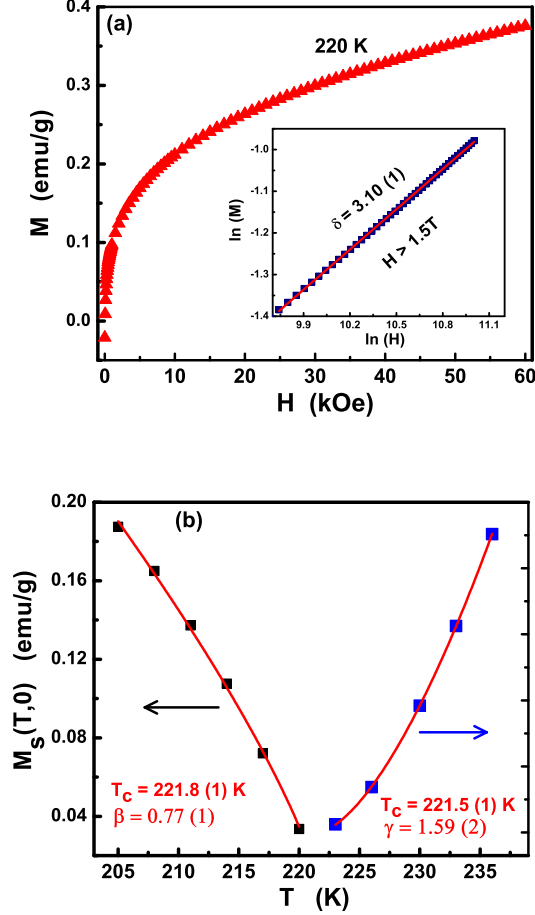


FIG. 5: (a) Magnetic isotherm  $M(H)$  at  $T = 220$  K near  $T_C$  to calculate the critical exponent  $\delta$  value. The inset shows the same plot on log-log scale with linear fit (solid red line). (b) The temperature dependence of spontaneous magnetization,  $M_S(T, 0)$  and the inverse initial susceptibility  $1/\chi_0(T)$ , along with power law (Eq. 1 and 2) fits (solid curves).

$$M = DH^{1/\delta}, \quad T = T_C \quad (3)$$

where  $\varepsilon = (T - T_C)/T_C$  is the reduced temperature;  $M_0$ ,  $h_0$  and  $D$  are the critical amplitudes. The reliable critical exponents have been determined using an iterative self-consistent method. Firstly, the  $\delta$  value has been determined using critical isotherm (CI) method (Eq. 3) by plotting the  $d \ln(H)/d \ln(M)$  against  $H$  for all the isotherms. The isotherm with its slope closest to zero corresponds to  $T = T_C$  and the intercept gives the  $\delta$  value. Accordingly,  $T_C = 220(3)$  K and  $\delta = 3.1(2)$  have been obtained. Figure 5(a) shows the magnetic isotherm at  $T = 220$  K (near  $T_C$ ), along with the same plot on log-log scale in the inset. Furthermore, the exact critical exponents follow the scaling law [26] in the critical region, according to which, the  $M(H, \varepsilon)/|\varepsilon|^\beta$  against  $H/|\varepsilon|^{1/\delta}$  plots lie on two universal branches below and above  $T_C$ . Using this approach, the  $\beta$  and  $\delta$  values are obtained as  $0.76(3)$  and  $3.0(1)$ , respectively, using  $T_C = 221$  K. The  $\gamma$

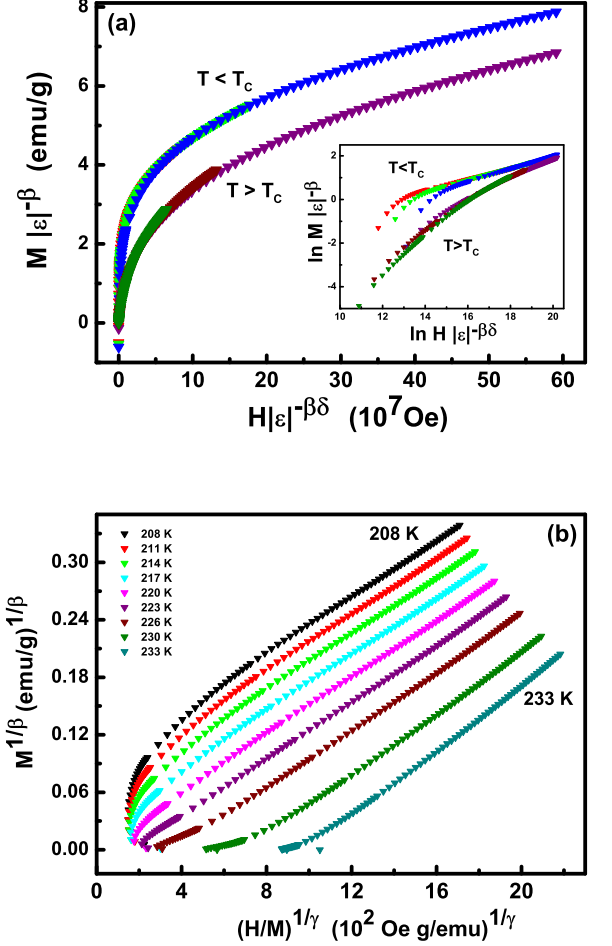


FIG. 6: (a) The scaling plots, below and above  $T_C$  using exponents from the modified Arrott plot analysis, along with same plot on log-log scale in the inset. (b) The Modified Arrott plot;  $M^{1/\beta}$  against  $(H/M)^{1/\gamma}$  with  $\beta = 0.77$  and  $\gamma = 1.59$ , at different temperatures around  $T_C$ .

value was determined as  $1.52(8)$  using the Widom scaling relation [27]. The obtained  $\beta$  and  $\gamma$  values were used as initial trial exponents for the MAP analysis. The linear extrapolation of the high field MAP data gives  $M_S(T)$  and  $1/\chi_0(T)$  values as intercept on  $M^{1/\beta}$  and  $(H/M)^{1/\gamma}$  axes, respectively. The  $M_S(T)$  and  $1/\chi_0(T)$  values were used for fitting of Eq. 1 and Eq. 2, respectively. The best fits to the data give  $\beta = 0.77(1)$  with  $T_C = 221.8(1)$  and  $\gamma = 1.59(2)$  with  $T_C = 221.5(1)$ , respectively [See Fig. 5(b)]. Moreover, the  $\delta$  value can be determined as  $3.06(4)$  using the Widom scaling relation.

The critical exponents from MAP method were examined using scaling theory with  $T_C = 221.5$  K. Figure 6(a) shows two universal branches for  $T > T_C$  and  $T < T_C$  respectively, which reflects the reliability of critical exponents. The modified Arrott plot reconstructed using above critical exponents is shown in Fig. 6(b). The MAP shows nearly parallel straight lines for high field region ( $H \geq 0.5$  T) in the vicinity of  $T_C$ . The low field non-linear behavior can be explained as a result of con-

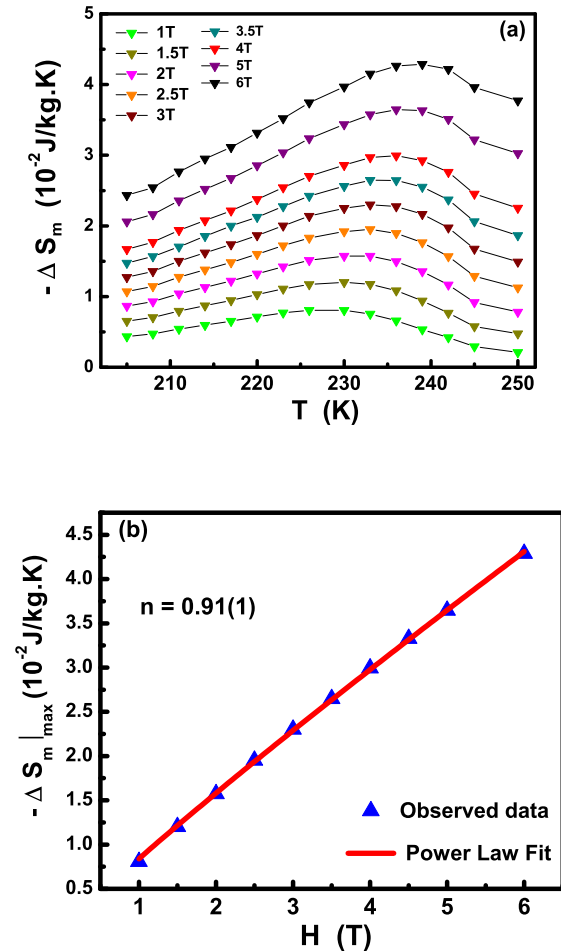


FIG. 7: (a) The change in magnetic entropy,  $-\Delta S_m$  (T) for different applied magnetic fields. (b) The magnetic field dependence of  $-\Delta S_m|_{max}$ , along with power law [ $-\Delta S_m|_{max} \propto H^n$ ] fit.

tribution from different magnetic domains, aligned along different directions [28].

The obtained critical exponents were further examined by analyzing the magneto-caloric effect in SIO across the phase transition. The change in magnetic-entropy ( $\Delta S_m$ ) is calculated using Maxwell relation [29] as

$$\Delta S_m = \left( \frac{\partial M}{\partial T} \right)_H \times H \quad (4)$$

Figure 7(a) shows the temperature dependence of the calculated  $-\Delta S_m$  for different fields. As, the  $-\Delta S_m$  is related to the change in magnetization with temperature, which is sharpest at the critical point, the  $-\Delta S_m$  plot shows broad peak around the critical temperature. The peak values of  $-\Delta S_m$  at the critical temperature for different fields are shown in Fig. 7(b). This data have been analyzed through power law,  $-\Delta S_m|_{max} \propto H^n$ , where  $n$  is the magnetic-ordering parameter. The best fit gives 'n'

TABLE I: Comparison of critical exponents of  $\text{Sr}_2\text{IrO}_4$  from MAP, CI and GP analysis with reported values and different theoretical models.

Material/Model	Ref	Method	$\beta$	$\gamma$	$\delta$
SIO	This Work	MAP	0.77(1)	1.59(2)	3.06(4)
SIO	This Work	CI	-	-	3.1(2)
SIO	This Work	GP	0.19(2)	-	-
SIO	[30]	$\mu\text{SR}$	0.20	-	-
SIO	[8, 33]	ND	0.18	-	-
SIO	[10]	XRMS	0.195	-	-
d:n=3:3					
Mean Field	[24]	Theory	0.5	1.0	3.0
3D Heisenberg	[24]	Theory	0.365	1.386	4.8
d:n=3:1					
3D Ising	[24]	Theory	0.325	1.24	4.82
d:n=2:2					
2D XY	[31]	Theory	0.23	-	-
d:n=2:1					
2D Ising	[32]	Theory	0.125	1.75	15.0

value as 0.91(1), which is consistent with  $n = 0.90$ , calculated using the theoretical relation,  $n = 1 + (\beta - 1) / (\beta + \gamma)$  [22, 29]. Thus, the magneto-caloric study further confirms the reliability of obtained critical exponent values.

The critical exponents determined from the magnetization, along with previously reported value and those for different known universality classes are listed in Table I. The comparison shows that obtained critical exponents for SIO do not fall into any known universality class. The universality classification is generally based on the dimensionality of lattice ( $d$ ) and spin ( $n$ ) system. Moreover, a two dimensional ( $d = 2$ ) nature of spin interaction is expected for layered SIO system, which has been experimentally verified recently [9, 30]. However, obtained  $\beta$  value is much higher than any  $d = 2$  models [31, 32] as well as previously reported  $\beta$  values from muon spin spectroscopy ( $\mu\text{SR}$ ) (0.20) [30], neutron diffraction (ND) (0.18) [8, 33] and XRMS (0.195) [10] techniques. Moreover, the obtained  $\beta$  value is unexpectedly large and can be linked with the presence of Griffiths phase (not pure PM phase) which exists up to much higher temperature,  $T_G = 279.0(5)$  K than magnetic ordering temperature,  $T_C = 221.5$  K. The similar unusual critical exponents have been earlier reported for Griffiths ferromagnets [15–17] via conventional critical phenomena techniques, due to the nonanalytic nature of Griffiths phase.

### C. Griffith phase analysis

As discussed in section III (A), negative downturn in  $1/\chi$  (T) plot much above  $T_C$  and higher experimental  $\mu_{eff}$  value confirm the presence of Griffiths singularity

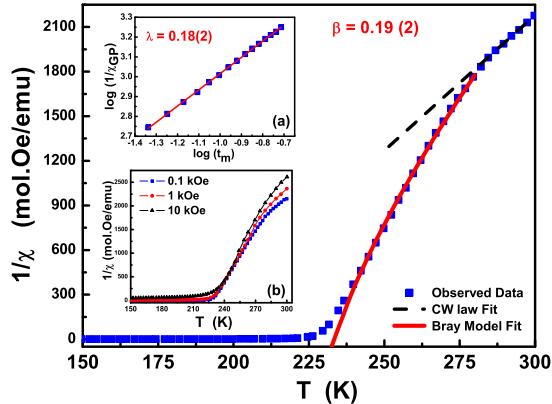


FIG. 8: The temperature dependence of  $1/\chi$  at 100 Oe. The solid line is Bray model fit [Eq. 8] to Griffiths phase, while the dashed line is Curie-Weiss law fit for reference. The inset (a) shows  $1/\chi_{GP}(T)$  versus  $t_m = (T - T_C^R) / T_C^R$  plot on log scale with power law [Eq. 5] fit. The inset (b) shows  $1/\chi(T)$  behavior with increasing magnetic fields from 100 Oe to 10 kOe.

in SIO. The low field magnetic susceptibility in the GP region,  $T_C < T \leq T_G$  follows the power law behavior [34],

$$\chi_{GP}^{-1}(T) \propto (T - T_C^R)^{1-\lambda}, \quad 0 < \lambda < 1 \quad (5)$$

where  $T_C^R$  is the critical temperature at which susceptibility tends to diverge and the exponent  $\lambda$  signifies the strength of disorder. The magnetic susceptibility at 100 Oe was analyzed in the framework of Eq. 5. The best fit gives the value of  $\lambda$  and  $T_C^R$  as 0.18(2) and 234.0(7) K, respectively. The fit to the data, plotted as  $1/\chi_{GP}(T)$  versus  $t_m = (T - T_C^R) / T_C^R$ , is shown in the inset (a) of Fig. 8. The non-zero less-than-unity exponent value further confirms the Griffiths singularity in SIO. The inset (b) of Fig. 8 shows the  $1/\chi(T)$  with increasing magnetic field, which provides further evidence for GP. One can clearly observe that negative downturn decreases with increasing magnetic field. The applied magnetic field favors the uniform magnetization and counteracts the disordered Griffiths phase. The suppression of disorder can also be seen from the trend of Griffiths exponent  $\lambda$ , which decreases from 0.18 (at 100 Oe) to 0.05 (at 10 kOe). The observed behavior is consistent with earlier reports on Griffiths ferromagnets [35, 36].

We have further analyzed GP using Bray model [13, 14], which considers the distribution of cluster sizes characterized by a susceptibility matrix in Griffiths ferromagnet. The inverse-susceptibility matrix eigenvalues,  $\eta/C$  follow the distribution,

$$p(\eta) \propto \eta^{-x} \exp[-A(T)/\eta] \quad (6)$$

where each  $\eta$  characterizes effective Curie-Weiss temperature difference,  $T - \theta_{eff}(T)$  for different cluster sizes.

The algebraic negative pre-factor was ignored in the original paper. However, later on, the eigenvalues distribution [Eq. 6] was confirmed with exponent value,  $x = 0.5$  for diluted Ising ferromagnet [37]. Moreover, the function  $A(T)$  vanishes at  $T = T_C^R$  and can be written as [12, 37],

$$A(T) = A_0 \left( \frac{T}{T_C^R} - 1 \right)^{2-2\beta} \quad (7)$$

where  $A_0$  is a constant and  $\beta$  is usual critical exponent for the system at its pure transition. As  $\eta = T$  for free spins, the average susceptibility can be written as,

$$\chi(T) = \frac{C}{\langle \eta \rangle} = C \frac{\int_0^T \eta^{-1} p(\eta) d\eta}{\int_0^T p(\eta) d\eta} \quad (8)$$

The fitting was performed by fixing the  $T_C^R$  value to 234.0 K obtained from power analysis Eq. (5). The best fit, shown by the solid line in Fig 8, gives  $\beta$ ,  $x$  and  $A_0$  values as 0.19 (2), 0.52 (2) and 299 (5) K, respectively. Surprisingly, the obtained  $\beta$  ( $= 0.19$ ) value is much smaller compared to MAP analysis ( $\beta = 0.77$ ). However, this value is in close agreement with reported values from  $\mu$ SR [30], ND [8, 33] and XRMS [10] measurements [See Table I]. The obtained  $\beta$  ( $= 0.19$ ) value along with Griffith phase confirms the 2D  $XYh_4$  universality class [38] with strong in-plane anisotropy, which shifts the  $\beta$  value from 2D XY ( $\beta = 0.23$ ) towards 2D Ising ( $\beta = 0.125$ ) interactions. Moreover, the consistency of  $\beta$  value from GP phase analysis with previous studies suggests Bray model as a possible tool to investigate the critical behavior for Griffiths ferromagnets.

Now, we will discuss possible origin of Griffith phase in SIO. Two main prerequisites for the realization of Griffiths ferromagnet are large magnetic anisotropy and intrinsic disorder. The canted antiferromagnet nature of SIO can result in large anisotropy between basal plane (easy axis) and  $c$ -axis (hard axis) [39]. While in-plane strong magnetic anisotropy below  $T_C$  has been observed via Raman scattering and Torque magnetometry measurements [40, 41], its existence well above  $T_C$  is established by Vale et al. [10]. Our critical exponent ( $\beta = 0.19$  corresponding to 2D  $XYh_4$  universality class) further supports such scenario of large magnetic anisotropy in SIO. The latter criterion for GP can be fulfilled by a number of intrinsic sources for local disorder in SIO. As shown in the right panel of Fig. 2, the alternate  $\text{IrO}_2$  planes rotate in clockwise and anticlockwise direction, respectively, forming a perfectly ordered structure. However, in real samples, the sequence of rotation in alternate layers is partially disordered as well as the rotation increases from  $11.36^\circ$  (at room temperature) to  $11.72^\circ$  (at 10 K) [7]. Depending on the amount of rotation, large variation in bending modes associated with the Ir-O-Ir bond angle can be observed [20], which leads to local distribution of magnetic exchange interaction and the formation of finite size clusters with short range magnetic order. Moreover, the neutron diffraction measurement has

shown the presence of two crystallographically twinned magnetic domains, which can inherently lead to formation of disordered magnetic clusters [33]. Apart from these, it has been shown that two competing ordered phases can lead to enhancement of Griffiths-like effects [42, 43]. Therefore, the competition between intralayer FM (in basal plane) and interlayer AFM (along  $c$ -axis) interactions in SIO can also give rise to Griffiths phase in SIO.

Next, we discuss a possible bearing of GP on the widely debated insulating phase in SIO. SIO has found several alternative descriptions: a Mott-Hubbard insulator [6], in which (on-site) Coulomb and exchange interactions are responsible for the gap formation, or a Mott insulator [1, 44], in which Coulomb interaction alone leads to gap formation, or a Slater insulator [45, 46], in which magnetic ordering causes an insulating gap. However, none of these descriptions individually provide a satisfactory explanation for the insulating nature and metal-insulator transition (MIT) in SIO. Recently, SIO has been termed as a “moderately correlated” insulator in which both Mott- and Slater-type behaviors [47, 48] coexist. Although the insulating gap closes at  $T_C$ , indicating Slater-type behavior, as observed by scanning tunneling spectroscopy, a pseudo-gap still exists at higher temperatures [46]. Moreover, the optical conductivity [49] and transport measurements [50] reveal the presence of an energy gap and bad metallic behavior in the paramagnetic phase. All these observations suggest a substantial contribution of the Mott-type correlation effects, which could have a possible origin in the GP observed here. Even though the long-range magnetic ordering vanishes above  $T_C$ , short-range magnetic interactions still persist in the GP, which could result in the formation of pseudo-gap, bad metallicity and continuous nature of the MIT, instead of a sharp transition in a Slater insulator. In addition, the dynamical mean-field theory calculations have shown that the pseudo-gap can be induced by short-range spin correlations in a Mott insulator [51]. Another possible origin of insulating state in SIO is that the gap begins to form in microscopically phase-separated regions above a bulk MIT temperature (close to  $T_C$ ), due to the presence of disorder in GP. Thus, a Mott-Anderson-Griffiths type MIT may be expected in SIO similar to the proposal by Biswas et al. [52]; according to which SIO can be treated as an inhomogeneous distribution of Mott insulating and Fermi liquid metal islands, forming an electronic GP. While disorder-driven Anderson localization have been previously suggested in SIO [46] and similar layered compound,  $\text{Ba}_2\text{IrO}_4$  [53], a complete determination of its contribution to the insulating phase would require a systematic inclusion of the disorder in SIO system.

Our study provides first experimental evidence for Griffith phase in SIO within the temperature range of  $T_C$  ( $= 221.5 \text{ K}$ )  $< T \leq T_G$  ( $= 279 \text{ K}$ ). The manifestation of

Griffith ferromagnetic phase have been observed in few recent experiments. For example, the XRMS measurements have shown that the magnetic correlations exist in paramagnetic phase above  $T_C$  [9, 10]. Moreover, a recent Raman study has reported the presence of two-magnon scattering well above  $T_C$  [54]. This provides the evidence for strong pseudospin excitations in paramagnetic state of SIO and the quenching of such fluctuations lead to sharp, dispersive magnon exciton modes below  $T_C$ . Still, further understanding of such novel magnetic phase in iridates demands more experimental and theoretical studies. The experimental techniques with high magnetic sensitivity (like electron spin resonance) are necessary to probe SIO near critical region. On the theoretical front, the models incorporating local disorder (like octahedral rotation), magnetic anisotropy and FM/AFM phase competition are needed to understand the GP and the insulating nature of SIO.

#### IV. CONCLUSION

In conclusion, the existence of Griffiths phase (GP) and its influence on critical phenomena in layered  $\text{Sr}_2\text{IrO}_4$  ferromagnet are reported in this work. The inverse susceptibility,  $1/\chi(T)$  shows downward deviation from CW behavior much above  $T_C$ , showing the existence of GP in SIO. The GP was confirmed from the power-law behavior of  $1/\chi(T)$  with less-than-unity exponent value,  $\lambda = 0.18(2)$ . The detailed isotherm analysis around  $T_C$  using modified Arrott plot reveals second order phase transition with critical parameters,  $\beta = 0.77(1)$ ,  $\gamma = 1.59(2)$  and  $\delta = 3.06(4)$  with  $T_C = 221.5(1) \text{ K}$ , in consistent with magneto-caloric study. However, the obtained  $\beta$  value is unrealistically large and has been associated with *ferromagnetic-Griffiths* phase transition. Further analysis of GP using Bray model gives reliable  $\beta$  [0.19(2)] value for  $\text{Sr}_2\text{IrO}_4$ . The obtained  $\beta$  value corresponding to 2D  $XYh_4$  universality class confirms the strong in-plane anisotropy, supporting presence of GP in the system. This study proposes Bray model as a possible tool to investigate the critical behavior for Griffiths ferromagnets via dc magnetization study. Furthermore, the study suggests that the GP plays an important role in Mott-type short-range correlations above  $T_C$  and disorder driven Anderson localization effects, which may be the possible origin of unconventional insulating nature of  $\text{Sr}_2\text{IrO}_4$ .

#### V. ACKNOWLEDGMENT

A. Rathi thanks University Grants Commission (UGC), India for providing the junior research fellowship (JRF) to carry out this research work and S. Perween thanks Department of Science and technology (DST), India for providing INSPIRE fellowship.

- 
- [1] B. J. Kim, H. Ohsumi, T. Komesu, S. Sakai, T. Morita, H. Takagi, and T. Arima, *Science* **323**, 1329 (2009).
- [2] F. Wang and T. Senthil, *Phys. Rev. Lett.* **106**, 136402 (2011).
- [3] X. Wan, A. M. Turner, A. Vishwanath, and S. Y. Savrasov, *Phys. Rev. B* **83**, 205101 (2011).
- [4] G. Cao, Y. Xin, C. S. Alexander, J. E. Crow, P. Schlottmann, M. K. Crawford, R. L. Harlow, and W. Marshall, *Phys. Rev. B* **66**, 214412 (2002).
- [5] M. K. Crawford, M. A. Subramanian, R. L. Harlow, J. A. Fernandez-Baca, Z. R. Wang, and D. C. Johnston, *Phys. Rev. B* **49**, 9198 (1994).
- [6] B. J. Kim, H. Jin, S. J. Moon, J. -Y. Kim, B. -G. Park, C. S. Leem, J. Yu, T. W. Noh, C. Kim, S. -J. Oh, J. -H. Park, V. Durairaj, G. Cao, and E. Rotenberg, *Phys. Rev. Lett.* **101**, 076402 (2008).
- [7] Q. Huang, J. L. Soubeyroux, O. Chmaissem, I. N. Sora, A. Santoro, R. J. Cava, J. J. Krajewski, and W. F. Peck, Jr., *J. Solid State Chem.* **112**, 355 (1994).
- [8] F. Ye, S. Chi, B. C. Chakoumakos, J. A. Fernandez-Baca, T. Qi, and G. Cao, *Phys. Rev. B* **87**, 140406 (2013).
- [9] S. Fujiyama, H. Ohsumi, T. Komesu, J. Matsuno, B. J. Kim, M. Takata, T. Arima, and H. Takagi, *Phys. Rev. Lett.* **108**, 247212 (2012).
- [10] J. G. Vale, S. Boseggia, H. C. Walker, R. Springell, Z. Feng, E. C. Hunter, R. S. Perry, D. Prabhakaran, A. T. Boothroyd, S. P. Collins, H. M. Rønnow, and D. F. McMorrow, *Phys. Rev. B* **92**, 020406 (2015).
- [11] R. B. Griffiths, *Phys. Rev. Lett.* **23**, 17 (1969).
- [12] M. B. Salamon, P. Lin, and S. H. Chun, *Phys. Rev. Lett.* **88**, 197203 (2002).
- [13] A. J. Bray and M. A. Moore, *J. Phys. C* **15**, L765 (1982).
- [14] A. J. Bray, *Phys. Rev. Lett.* **59**, 586 (1987).
- [15] W. Jiang, X. Z. Zhou, G. Williams, Y. Mukovskii, and K. Glazyrin, *Phys. Rev. Lett.* **99**, 177203 (2007).
- [16] T. L. Phan, S. G. Min, S. C. Yu, S. K. Oh, *J. Magn. Mater.* **304**, e778 (2006).
- [17] M. Triki, E. Dhahri, E. K. Hlil, *J. Solid State Chem.* **201**, 63 (2013).
- [18] N. S. Kini, A. M. Strydom, H. S. Jeevan, C. Geibel, and S. Ramakrishnan, *J. Phys.: Condens. Matter* **18**, 8205 (2006).
- [19] I. N. Bhatti, R. Rawat, A. Banerjee and A. K. Pramanik, *J. Phys.: Condens. Matter* **27**, 016005 (2014).
- [20] S. Chikara, O. Korneta, W. P. Crummett, L. E. DeLong, P. Schlottmann, and G. Cao, *Phys. Rev. B* **80**, 140407 (2009).
- [21] W. Jiang, X. Z. Zhou, and G. Williams, Y. Mukovskii, and K. Glazyrin, *Phys. Rev. B* **77**, 064424 (2008).
- [22] T. A. Ho, T. D. Thanh, Y. Yu, D. M. Tartakovsky, T. O. Ho, P. D. Thang, A. Le, T. Phan, and S. C. Yu, *J. Appl. Phys.* **117**, 17D122 (2015).
- [23] A. Arrott, *Phys. Rev.* **108**, 1394 (1957).
- [24] S. N. Kaul, *J. Magn. Mater.* **53**, 5 (1985).
- [25] S. Banerjee, *Phys. Lett.* **12**, 16 (1964).
- [26] A. Arrott, J. E. Noakes, *Phys. Rev. Lett.* **19**, 786 (1967).
- [27] B. Widom, *J. Chem. Phys.* **43**, 3892 (1965).
- [28] A. K. Pramanik and A. Banerjee, *Phys. Rev. B* **79**, 214426 (2009).
- [29] V. Franco, J. Blazquez, and A. Conde, *Appl. Phys. Lett.* **89**, 222512 (2006).
- [30] M. Miyazaki, R. Kadono, M. Hiraishi, A. Koda, K. M. Kojima, K. Ohashi, T. Takayama, and H. Takagi, *Phys. Rev. B* **91**, 155113 (2015).
- [31] J. Als-Nielsen, S. T. Bramwell, M. T. Hutchings, G. J. McIntyre, and D. Visser, *J. Phys.: Condens. Matter* **5**, 7871 (1993).
- [32] F. Kagawa, K. Miyagawa, and K. Kanoda, *Nature* **436**, 534 (2005).
- [33] C. Dhital, T. Hogan, Z. Yamani, C. de la Cruz, X. Chen, S. Khadka, Z. Ren, and S. D. Wilson, *Phys. Rev. B* **87**, 144405 (2013).
- [34] A. H. Castro Neto, G. Castilla, and B. A. Jones, *Phys. Rev. Lett.* **81**, 3531 (1998).
- [35] H. S. Nair, D. Swain, N. Hariharan, S. Adiga, C. Narayana, and S. Elizabeth, *J. Appl. Phys.* **110**, 123919 (2011).
- [36] W. Jiang, X. Z. Zhou, G. Williams, Y. Mukovskii, and K. Glazyrin, *Phys. Rev. B* **76**, 092404 (2007).
- [37] A. J. Bray and D. Huifang, *Phys. Rev. B* **40**, 6980 (1989).
- [38] A. Taroni, S. T. Bramwell, and P. C. W. Holdsworth, *J. Phys.: Condens. Matter* **20**, 275233 (2008).
- [39] Y. Hong, Y. Jo, H. Y. Choi, N. Lee, Y. J. Choi, and W. Kang, *Phys. Rev. B* **93**, 094406 (2016).
- [40] Y. Gim, A. Sethi, Q. Zhao, J. F. Mitchell, G. Cao, and S. L. Cooper, *Phys. Rev. B* **93**, 024405 (2016).
- [41] L. Fruchter, D. Colson and V. Brouet, *J. Phys.: Condens. Matter* **28**, 126003 (2016).
- [42] C. Magen, P. A. Algarabel, L. Morellon, J. P. Araújo, C. Ritter, M. R. Ibarra, A. M. Pereira, and J. B. Sousa, *Phys. Rev. Lett.* **96**, 167201 (2006).
- [43] J. Burgy, M. Mayr, V. Martin-Mayor, A. Moreo, and E. Dagotto, *Phys. Rev. Lett.* **87**, 277202 (2001).
- [44] G. Jackeli and G. Khaliullin, *Phys. Rev. Lett.* **102**, 017205 (2009).
- [45] R. Arita, J. Kunes, A.V. Kozhevnikov, A. G. Eguiluz, and M. Imada, *Phys. Rev. Lett.* **108**, 086403 (2012).
- [46] Q. Li, G. Cao, S. Okamoto, J. Yi, W. Lin, B. C. Sales, J. Yan, R. Arita, J. Kuneš, A. V. Kozhevnikov, A. G. Eguiluz, M. Imada, Z. Gai, M. Pan, and D. G. Mandrus, *Sci. Rep.* **3**, 3073 (2013).
- [47] D. Hsieh, F. Mahmood, D. H. Torchinsky, G. Cao, and N. Gedik, *Phys. Rev. B* **86**, 035128 (2012).
- [48] H. Watanabe, T. Shirakawa, and S. Yunoki, *Phys. Rev. B* **89**, 165115 (2014).
- [49] S. J. Moon, H. Jin, W. S. Choi, J. S. Lee, S. S. A. Seo, J. Yu, G. Cao, T. W. Noh, and Y. S. Lee, *Phys. Rev. B* **80**, 195110 (2009).
- [50] M. Ge, T. F. Qi, O. B. Korneta, D. E. De Long, P. Schlottmann, W. P. Crummett, and G. Cao, *Phys. Rev. B* **84**, 100402 (2011).
- [51] B. Kyung, S. S. Kancharla, D. Sñchal, A. -M. S. Tremblay, M. Civelli and G. Kotliar, *Phys. Rev. B* **73**, 165114 (2006).
- [52] A. Biswas, K. Kim, and Y. H. Jeong, *J. Appl. Phys.* **116**, 213704 (2014).
- [53] H. Okabe, N. Takeshita, M. Isobe, E. Takayama-Muromachi, T. Muranaka, and J. Akimitsu, *Phys. Rev. B* **84**, 115127 (2011).
- [54] H. Gretarsson, N. H. Sung, M. Hppner, B. J. Kim, B. Keimer, and M. Le Tacon, *Phys. Rev. Lett.* **116**, 136401 (2016).